An Investigation of the Stresses Causing the Spontaneous Delamination of Titanium-Platinum Bilayers Leading to The Formation of Nanogaps

Thesis by

Afnan AlBatati

In Partial Fulfillment of the Requirements

For the Degree of

Master of Science

King Abdullah University of Science and Technology, Thuwal,

Kingdom of Saudi Arabia

July 2020

EXAMINATION COMMITTEE

The thesis of Afnan AlBatati is approved by the examination committee.

Committee Chairperson: Prof. Thomas Anthopoulos

Committee Members: Prof. Frédéric Laquai, Prof. Vincent Tung, Prof. Gilles Lubineau

ABSTRACT

An Investigation of the Stresses Causing the Spontaneous Delamination of Titanium-Platinum Bilayers Leading to The Formation of Nanogaps

Afnan AlBatati

Adhesion lithography has been used to pattern nanogaps between two electrodes of the same or different metals onto a substrate. Patterning Al and Ti/Pt bilayer electrodes have been shown to form nanogaps leaving behind relatively consistent nanogaps of less than 12 nm between the electrodes. These nanogaps are formed without the need for adhesion lithography due to the bilayer spontaneously delaminating from the aluminum electrodes, In this study, the stresses in the Ti/Pt bilayer are investigated to determine the amount of stress required for delamination and the properties causing it. The goal is to recreate this stress mechanism in other patterned metals such as Au and Al. Heat cycling is used to induce high stress in other metal electrode combinations in an attempt to induce spontaneous delamination in Al and Au but fails up to 310°C annealing temperature. Theoretical methods are used to determine the stress: searching for an appropriate mathematical model and using finite element analysis in ABAQUS software to create a simulation of the delaminating Ti/Pt bilayer. The stress is found to be caused by the residual stresses in platinum and the high energy e-beam deposition method. An experimental value for the stress and the ability to recreate it in other metals remains elusive.

ACKNOWLEDGEMENTS

I would like to thank Professor Thomas Anthopoulos for giving me the opportunity to conduct this research. His big picture perspective is inspirational and his guidance invaluable. Thank you to the LAMA group members for their endless optimism and support. A special thank you to Kalaivanan Loganathan and Hendrik Faber for their mentorship and patience with all my questions. Thank you to Akmaral Seitkhan for her skills using the SEM. Thank you to Professor Gilles Lubineau and Xiaole Li for their expertise and mentorship in mechanical stress simulation. Thank you to KAUST, my home, for providing me the opportunity to study my bachelor's degree at the wonderful University of Wisconsin-Madison as a part of the KAUST Gifted Student Program and accepting me back to continue my master's and PhD. Last but certainly not least I would like to thank my friends and family for their love and support through the good times and the bad. I really could not have done it without you all.

TABLE OF CONTENTS

Page

LIST OF ABBREVIATIONS

A-lith	Adhesion lithography
AFM	Atomic Force Microscopy
Al	Aluminum
Au	Gold
CTE	Coefficient of Thermal Expansion
Cu	Copper
DI	Deionized
FEA	Finite Element Analysis
IPA	Iso-Propyl Alcohol
Mo	Molybdenum
Nb	Niobium
ODPA	Octa-Decyl Phosphonic Acid
Pt	Platinum
SAM	Self-Assembled Monolayer
SEM	Scanning Electron Microscopy
Si	Silicon
Ti	Titanium
W	Tungsten

LIST OF SYMBOLS

α	Coefficient of linear thermal expansion
E	Young's Modulus
v	Poisson's ratio
R	radius of curvature in Stoney's equation
ρ	radius of curvature in Timoshenko's equation
σ	stress

LIST OF ILLUSTRATIONS

LIST OF TABLES

Chapter 1: Introduction

1.1 Nanogaps

As technology weaves its way into the fabric of our daily life, the need for smaller and more flexible electronics that can be cheaply produced and easily integrated into our lives increases. Microprocessors are reaching the limits of the infamous Moore's law, which states that the number of transistors on an integrated circuit doubles every two years. Transistors are now on the order of 10 nanometers in size and are reaching the physical limits defined by the silicon parts [1]. The silicon channel in a transistor has become thin enough that any further decrease in thickness would result in electrons tunneling through the material. A change in how we build devices is necessary. Molecular-based devices present many advantages for electronic devices; they can be manufactured at a lower cost, have lower power consumption and higher efficiency, and can utilize optical and electrical properties unique to their dimensions.

Nanogap electrodes allow us to create these minute devices and exploit the unique properties present at the molecular level. They can be used to make transistors small enough to possibly integrate billions of them. Nanogaps are nano-scale gaps between two metal electrodes, ideally less than 10 nm in size. Bringing metals in such proximity allows for electronic interaction such as devices that operate using electronic tunneling, photonic interaction utilizing the inherent properties of the metals, mechanical interactions based on the motion of one or both electrodes, and molecule-trapping and detection for use in molecular sensors [2].

Nanogaps can be created using a top-down or a bottom-up approach. A top-down approach involves the creation of nano-features from the reduction of bulk materials. Top-down approaches such as scanning tunneling microscopy (STM) have been used initially to create the nanogap by bringing the electrodes in proximity or using a tool to cut a gap in a metal film. These methods present several limitations, such as the requirement of using large, expensive tools, the inability to accurately measure the gap size while creating it, and most importantly, the inability to create more than one gap at a time, providing a time and mass production limitation.

A bottom-up approach takes on building of nano-features from atoms. This is seen in nanowire growth methods [3-4]. Bottom-up approaches have proven more effective in planarly patterning nanogaps during the creation of the devices. The planar geometry allows high-density integration, the patterning of different metal electrodes, and faster and cheaper production. A bottom-up approach is more favorable for the creation of nanogaps, which are scalable and easy to deploy in large-area manufacturing.

In this project, nanogaps are patterned between two co-planar metal electrodes onto a substrate using adhesion-lithography. When the first metal used is aluminum and the second is a titanium/platinum bilayer, a phenomenon is observed where nanogaps are formed spontaneously, removing the need for adhesion lithography. Adhesion lithography (a-lith) is the application of an adhesive layer on top of the substrate, such as liquid glue or tape, and the mechanical peeling of it [5-6]. The size of the nanogaps formed when the top layer of metal is peeled off is subject to the shear force with which it was removed [6]. This leads to variation in the sizes of the nanogaps caused by user error. However, when the nanogaps are spontaneously formed, the top metal layer delaminates

uniformly through intrinsic stress causing a more uniform formation of gaps. The nanogaps thus form in smaller and more uniform sizes because significantly less or almost no shear force is used, and the uniform stress distribution across the substrate, respectively. Spontaneous delamination occurs only when platinum is used as the second metal. Through this work, we aim to explore the stresses driving the self-peeling mechanism and use similar stress mechanisms to pattern nanogaps using other metal electrodes such as gold and aluminum. These tools will simplify the fabrication process and potentially create more consistently sized nanogaps since they are not subject to an external peeling or shear force. The advantage of adhesion lithography over previous methods of nanogap formation is the ability to pattern different metal electrodes simultaneously and the scalability of the process.

1.2 Stress in Thin Metal Films

Stress in thin metal films has often been an undesirable physical phenomenon that causes the buckling or delamination of films on a substrate ultimately causing the failure of microsystems and devices. More recently, the effects of stress have been used to the advantage of creating novel structures in micro or nano-systems [7-11]. The rolling of stressed thin films lead to the creation of nanotubes and various other shapes that would be difficult to create mechanically. The formation of these shapes can be used as a trigger mechanism, as a structural design in a microsystem, or even for aesthetic purposes.

Traditionally, the bending of a substrate caused by stresses in the coating film is calculated using classical bending theory. Stoney developed an equation that uses the radius of the substrate’s curvature to find the stress [12]; Timoshenko adapted these equations for stress calculations of a bimetallic strip used for thermostats [13]. Since

then, these equations have been further modified for various applications [14-17]. There are measurement systems that use Stoney's equation to calculate the stress in a substrate placed in a chamber such as the FLX Stress Measurement System. Finite element analysis (FEA) can be used to create a theoretical model of the system.

Chapter 2: Background & Theory

2.1 Fabrication

2.1.1 Evaporation Deposition

Thermal evaporation is used to deposit materials onto a substrate suspended in a vacuum chamber. A crucible containing the source material is heated until its evaporation point, and the adatoms land on the surface of the substrate, forming a film. The deposition rate is monitored via a quartz sensor to measure the thickness of the deposited layer. Thermal evaporation is used to deposit materials that have a relatively low evaporation point.

Electron-beam evaporation is a deposition method used to deposit materials onto a substrate suspended in a vacuum chamber. A high energy electron beam is directed at the source material to evaporate it. This deposition method is used to deposit materials with a relatively high vaporization temperature. The high energy electrons provide enough energy to heat the source and the energy is localized, so the chamber, and substrate are not affected by the heat.

2.1.2 Self-Assembled Monolayer

Self-assembled monolayers (SAM) are crucial for the development of nanogaps using adhesion lithography (a-lith). Self-assembled monolayers are small organic molecules, a few nanometers in length that are made up of a head group, a tail, and a functional end group. These parts contain different molecular structures and serve different functions. The head group selectively adsorbs onto the surface of a material, causing the SAM molecules to organize onto the surface of the select material with minimal interaction between the individual SAM units. The functional end group can then be used to adhere

to another material if they chemically bond. It can also be specifically selected so that it does not bond with another material effectively, creating an insular layer that can cause poor adhesion and thus helps to remove the subsequently deposited layers. SAMs are deposited from a solution where the substrate is immersed in a dilute SAM solution and allowed to form at room temperature over 12 to 72 hours [18-19]. The molecules organize onto the surface of the material and are relatively packed due to the weak Van der Waals forces between the individual units.

2.1.3 Adhesion Lithography

Adhesion lithography is a simple fabrication method that allows the formation of nanogaps. Films are deposited sequentially using lithographic methods such as photolithography and masking.

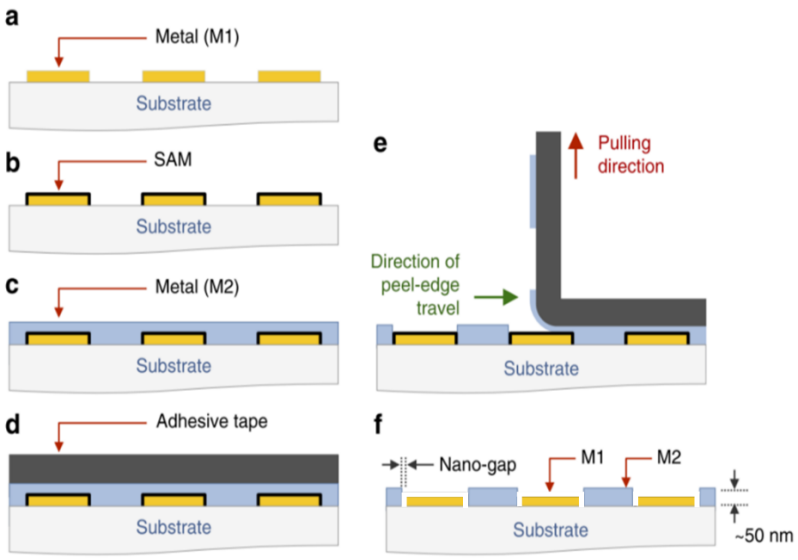

Figure 2.1: Schematics of the formation of nanogaps via adhesion-lithography. (a) The deposition of the first metal (M1) electrodes. (b) Deposition of the self-assembled monolayer (SAM) onto M1. (c) The second metal (M2) is deposited everywhere. (d) An adhesive tape or

glue is placed on top of M2, then (e) it is pulled off. (f) M2 is removed from where it interfaces with the SAM, and nanogaps are formed between M1 and M2. Taken from [6].

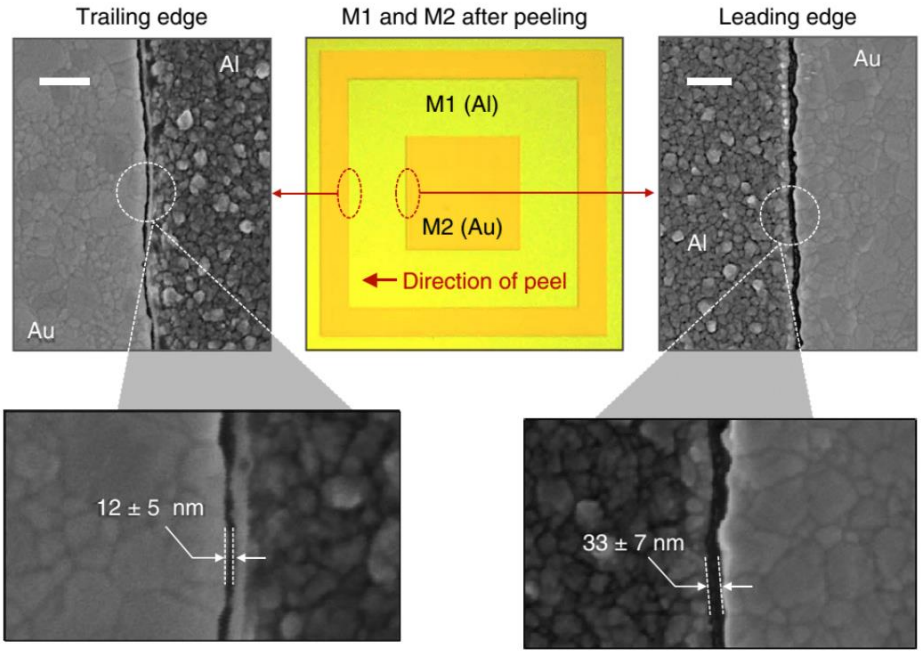

Figure 2.2: Micrographs (top) of Al first metal electrode and Au second metal electrodes and scanning electron microscope images of the nanogap formed after adhesion lithography (bottom). Scale bars are 250 nm. Taken from [6].

In the original process, nanogaps are formed using adhesion lithography [5-6]. The first metal electrodes are patterned onto a 1.1 mm thick Borofloat glass substrate using photolithography (figure 2.1a). In this work, the first metal is a 100 nm aluminum. A self-assembled monolayer (SAM) of octadecyl phosphonic acid (ODPA) is deposited selectively onto the aluminum layer without adhering to the glass substrate (figure 2.1b). A second metal is then deposited uniformly onto the substrate (figure 2.1c). In the areas where the second metal and the SAM interface, there is little to no adhesion. The second

metal is deposited via either thermal evaporation (Al or Au) or electron-beam evaporation (Ti and Pt) and is 100 nm thick. An adhesive layer is then spread uniformly onto the surface of the second metal, allowed to dry, and then slowly peeled off (figure 2.1d-e). The second metal is completely removed from on top of the SAM-coated first metal creating a uniform planar patterning of the first and second metal electrodes. The SAM is then rinsed off in isopropanol (IPA) for a minute. Since the SAM covers the top and sides of the first metal layer, a nano-sized gap is developed between the metals (figure 2.1f). The size and size variation of this gap is influenced by the shear force used to peel off the adhesion layer and the direction of peeling relative to the location of the second metal (figure 2.2). Increased force and pulling against the direction of the second metal causes larger nanogaps [6].

2.2 Stress Analysis

2.2.1 Background

A stressed thin film can be under either tensile or compressive stress. Tensile stress refers to the force pulling a material outward and keeping it in tension, whereas compressive stress is a force pushing into the material. In thin films, intrinsic stresses originate at the surfaces and interfaces of the films. This is due to the surface reconstruction and lattice mismatch of the thin film. At relatively small thicknesses, surface reconstruction can cause enough force to bend films. In films that buckle and cause pockets on the surface, there is tensile stress at the top surface of the film and compressive stress in the bottom interface. In films that roll or peel off, there is compressive stress on the top surface and tensile stress in the bottom interface. Zang et al. modeled the stresses causing the rolling of Ge/Si films into nanotubes (figure 2.3). In literature discussing the stresses in thin

films and in calculations such as Stoney's equation, the stress-causing buckling is generally referred to as compressive stress, and the stress-causing rolling is referred to as tensile stress.

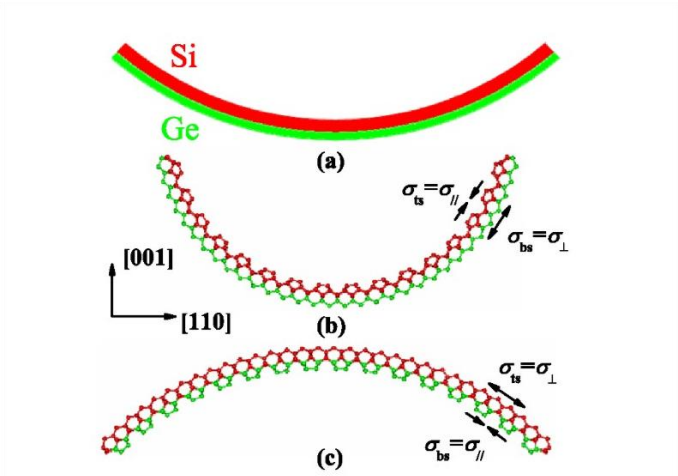

Figure 2.3: Diagram of the tensile and compressive stresses causing the bending of Ge/Si bilayer films. Taken from [20].

The cause of stress in materials is classified as either intrinsic or extrinsic. Extrinsic stress is caused by external factors, such as an external force or temperature. Many factors can cause intrinsic stress, and the source is often difficult to pinpoint [21]. Nevertheless, experimental and theoretical methods can be used to quantify the stress in a physically deformed film or substrate. When the metal peels off the substrate's surface and rolls into tubes, the rolling diameter can be used to determine the amount of stress using mathematical models. Finite element analysis can be used to simulate the peeling mechanism. Based on a study published in 2012 by Lee et al., where they measured the

stress causing the formation Ti/Pt microtubes, the measured stress should be 700-800 MPa [7].

Table 2.1: Material constants of metals used to create nanogap electrodes.

	Melting Point (°C)	Thermal Expansion Coefficient, α (1/°C)	Atomic mass (u)	Young's Modulus, E (GPa)	Poisson's Ratio, ν
Aluminum	660.3	24×10^{-6}	26.981539	69	0.334
Titanium	1668	$8.5\text{-}9 \times 10^{-6}$	47.867	113.8	0.32
Platinum	1768	9×10^{-6}	195.084	169	0.39
Gold	1064	14×10^{-6}	196.96657	79	0.415

Material properties affect the intrinsic stress distribution and effects on the bulk material. Stresses in thin metal films range from 10 to 5000 MPa [21]. It is usually tensile stress with refractory metals such as Mo, Nb, and W, displaying high values of stress and soft metals such as Al, Au, and Cu, displaying low values of stress. The coefficient of thermal expansion (CTE) of a material is a measurement of physical change with a change in temperature. Materials with a high CTE experience more stress effects due to significant temperature changes. Since our devices are deposited at approximately room temperature, the films are only subjected to large temperature changes during deposition. Ti and Pt have nearly identical CTEs at ~9 E-6 /°C and similarly high melting points (table 2.1).

Temperature plays an essential role in the development of stress in our thin metal films. It is the only extrinsic stress our devices are subject to. The substrates can be heated during deposition or annealed post-processing. Heating the substrate or chamber during deposition increases diffusion and coalescence causing Frank-van der Merwe (layer) growth. The resulting film would have lower residual stress and is undesirable. Heating

the substrate post-deposition, however, increases the stresses in the metal films. Research has shown that stress can be induced in thin films by using heat cycles [22-24].

2.2.2 Heat Cycles

One method of increasing stress in thin films is by applying extrinsic stress through annealing. Researchers have found that applying heat cycles to Al, Au, and Ag films increases the stress [22-24]. Heat cycling is a method where a material is heated to a certain temperature then allowed to cool to room temperature. It is heated again and allowed to cool; this process is usually repeated 3-4 times with the most significant change in stress occurring after the first cycle. Hodge et al. demonstrated an increase of ~50 MPa in Au films and ~140 MPa for Al films deposited on a silicon substrate heated from room temperature to approximately 200°C [22].

2.2.3 Stoney's Equation

The first quantitative analysis of the stress in a film was developed in 1909 by Stoney [12]. The equation uses the radius of a substrate's curvature to determine the stress in the coating films,

$$\sigma = \frac{E_s h_s^2}{6(1-v_s)h_f}\left(\frac{1}{R} - \frac{1}{R_0}\right) \quad (1)$$

where σ is stress in the film, E_s is the Young's modulus of the substrate, v_s is Poisson's ratio of the substrate, h is the thickness, and R is the radius of curvature after film deposition, and R_0 is the initial radius of curvature. Stoney's equation does not correctly measure the stress in our system due to several factors. The main obstacle is that our

Ti/Pt film delaminates from the surface of the octadecyl phosphonic acid (ODPA) SAM-coated Al. To overcome this in the calculation, one can assume that Ti is the substrate, and Pt is the film. This does not work because the accuracy of Stoney's equation falters as films become too thick relative to the substrate. The error becomes significant when the coating thickness is 5% or more the thickness of the substrate [12]. The thickness ratio between the film and substrate should be less than 0.1. Above 0.2, the difference causes significant error [17]. Another solution is to assume that the stress is continuous throughout the Ti/Pt layer. That way, it can be measured where it still adheres to the surface of our Borofloat glass substrate. This was attempted using the FLX-2320.

2.2.4 Timoshenko's Equation

Stoney's equation has been adapted and modified for various applications. Timoshenko [13] adapted Stoney's equation for using known parameters and the change in temperature to measure the radius of curvature. This is used to determine the stress resulting from heating,

$$\rho = \frac{t\cdot[3\cdot(1+m)^2+(1+m\cdot n)\cdot\left(m^2+\frac{1}{m\cdot n}\right)]}{6\cdot(\alpha_2-\alpha_1)\cdot(T_h-T_c)\cdot(1+m)^2} \quad (2)$$

where ρ is the radius of curvature (the same parameter as R in Eq.(1)), t is the total thickness of both films t_1 and t_2, $m = \frac{t_1}{t_2}$ is the ratio of thicknesses, $n = \frac{E_1}{E_2}$ is the ratio of the Young's moduli of both films, T_c and T_h are the hot and cold temperatures, α_1 and α_2 are the CTEs of the two metals. α_2 is assumed to be larger than α_1. Timoshenko's equation was developed for macroscopically thick films, J. Zang and F. Liu modified the equation in 2008 for use in bimetal systems with nanometer scale thickness [16]. The

modified formula in Equation 3 allows the calculation of radius of curvature from the difference in stress between the top and bottom surfaces of the bimetal strip.

$$\rho = \frac{6(E_1 \varepsilon_m t_1)+6(G_1 \sigma_{ts0} - G_2 \sigma_{bs0})}{E_2 t^2} \gamma \tag{3}$$

$$G_1 = \frac{1+2n+mn^2}{1+n}, \qquad G_2 = \frac{1+2mn+mn^2}{1+n} \tag{4}$$

$$\gamma = \frac{(1+n)^3}{1+4mn+6mn^2+4mn^3+m^2n^4} \tag{5}$$

Chapter 3: Experimental Methods

3.1 Fabrication

3.1.1 Substrate Preparation

1x1” Borofloat glass substrates of 1.1 mm thickness are cleaned in preparation for material deposition. The substrates are first placed in deionized (DI) water and sonicated for 15 minutes. Then they are dried with nitrogen gas and placed in an acetone bath and sonicated for 15 minutes. This is followed by an isopropanol (IPA) bath sonicated for 15 minutes then dried with nitrogen gas. Plasma cleaning is avoided due to its interference with the ODPA SAM selective bonding mechanism, allowing it to bond to the glass substrate.

3.1.2 Photolithography

Photolithography is a method used to pattern layers of material onto a substrate. An advantage of photolithography over shadow-masking is the accuracy of the edge profile. A sharp edge profile is important to the formation of nanogaps since it can dramatically affect the nanogap’s quality and consistency. A 100 nm aluminum layer is first deposited onto the glass substrate using thermal evaporation. A photoactive material, photoresist, is then deposited onto the Al-coated glass substrate and then covered with a dark-field mask design of our desired circle pattern (figure 3.1). The combination is then subjected to UV light where the exposed photoresist hardens and the rest of it can be removed. The unreacted photoresist is removed and then the underlying Al can be chemically etched away. Using a chemical specifically designed to etch photoresist, the rest of the hardened photoresist can be removed, leaving behind the circular aluminum pattern.

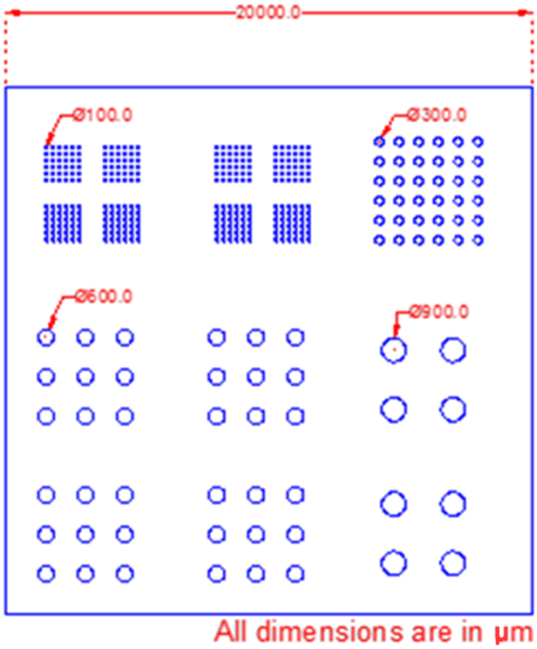

Figure 3.1: Mask design for circular electrodes of 100, 300, 600, and 900 µm diameters.

The successful formation of planar nanogaps by a-lithography or self-peeling is consistent regardless of the mask design used to create the samples. In this work, we use a circle pattern mask containing 100, 300, 600, and 900 µm diameter circles (figure 3.1).

3.1.3 SAM Deposition

The self-assembled monolayer (SAM) of octadecylphosphonic acid (ODPA) is created by mixing 7.8 mg (1mM) of ODPA in 30 mL of isopropanol (IPA) for 5 to 20 hours at room temperature until the ODPA is fully dissolved. The substrate with the patterned Al is then submerged in the solution for 20 hours at room temperature. The ODPA molecule is a few nm in length and comprises a phosphonic acid head group and an 18-carbon alkyl chain [25]. The phosphonic head group attaches onto the aluminum because of the interaction of the head group with the metal oxide layer. Substrates are then rinsed with

IPA and dried with nitrogen gas to remove excess physically adsorbed ODPA. Substrates are then annealed on a hot plate at 80°C for 15 minutes.

3.1.4 Self-Peeling

The self-peeling devices are fabricated in much the same way as the devices in the a-lith process. After the deposition of 100 nm of Al as the first metal and the ODPA SAM, which selectively bonds onto the surface of Al (figure 3.2a-b). Electron-beam evaporation is then used to deposit 5 nm of Ti then 95 nm of Pt sequentially at a high vacuum of 2 E-6 Torr in an unheated chamber (figure 3.2c). The Ti/Pt 5/95 nm bilayer spontaneously delaminates immediately after deposition and small flakes and rolls of the delaminated material are observed on the surface of the devices (figure 3.2d). Due to the self-peeling, a separate peeling step is not required. The flakes can be removed with some air pressure or agitation in acetone leaving behind nanogaps between the Al and Pt electrodes on the order of 10 nm (figure 3.2e). Since there is no external force used to peel the second metal, the nanogap sizes seem to be more consistent and smaller than those developed using a-lithography.

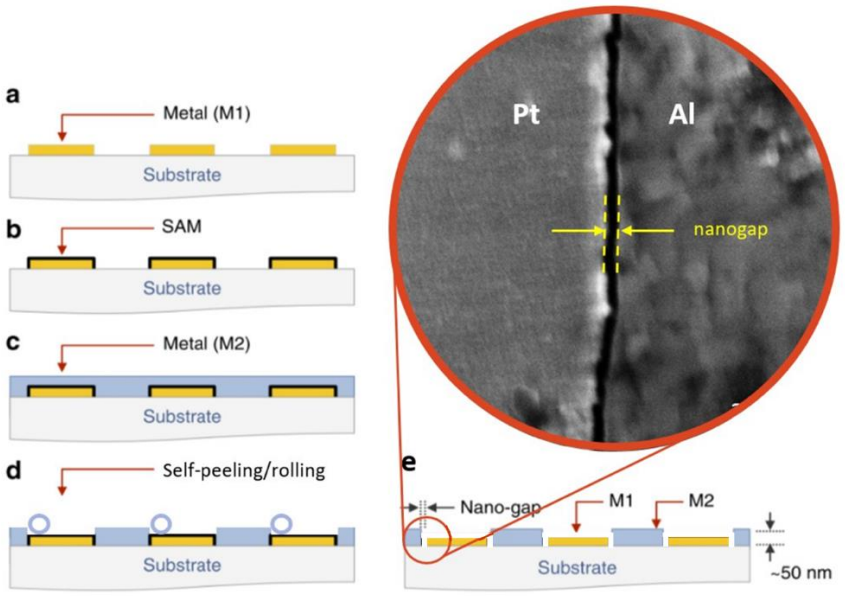

Figure 3.2: Procedure for the formation of nanogaps by self-peeling. (a) The first metal (M1) aluminum electrode is deposited onto a substrate then (b) the ODPA self-assembled monolayer (SAM) is deposited onto M1. (c) The second metal (M2) titanium/platinum bilayer is deposited everywhere where (d) the bilayer self-peels off from the SAM surface leaving (e) nanoscale gaps between the two metals as shown in the SEM image.

3.2 Characterization

3.2.1 Optical Microscopy

A Zeiss Microscope Axio Observer Z1M was used to obtain micrographs of the flakes at 5x, 10x, and 20x magnification objectives.

3.2.2 Atomic Force Microscopy

An NT-MDT Next Atomic Force Microscopy (AFM) is used to create a topographical image of a sample. A whisker tip cantilever with a 5° angle tip is used in tapping mode at a 90-degree angle to the surface. The force between the tip and the surface is measured by measuring the cantilever's deflection using position-sensitive four-quadrant photodiodes. The back of the cantilever contains a small mirror which will deflect a laser beam to the photodiodes [26]. The accompanying Nanoscope software is used to analyze the data collected from the AFM.

3.2.3 Scanning Electron Microscopy

Scanning electron microscopy (SEM) is a method of light microscopy that uses an electron beam to scan the surface of a sample contained in a vacuum chamber. SEM can obtain images up to 30,000X magnification and has a high depth of field so the topography of the surface and artifacts of the surface can be imaged as well. A FEI Helios G4 UX was used to obtain close-up images of the flakes and images angled up to 60°. The flakes' diameters were also measured using the SEM, providing us with the radius of curvature of the flakes.

3.2.4 FLX-2320 Stress measurement system

The FLX Stress Measurement System seen in Figure 3.3 uses two lasers at 670 nm and 780 nm and 4 mW to scan a substrate's surface before and after a film is deposited onto it. The lasers raster the surface and measure the change in curvature radius caused by the stress in the film. The interior chamber supports circular wafers of 8", 6", and 4" diameters. The resting surface for the substrate doubles as a hot plate for in-situ heating

and stress-temperature dependence analysis. The accompanying software uses the collected radius of curvature measurements and known temperature values and applies Stoney's equation to calculate the stress in the film.

Figure 3.3: The FLX-2320 Stress Measurement system wafer chamber and accompanying software.

3.3 Simulation

3.3.1 Finite Element Analysis

Finite element analysis (FEA) is a computational method used to analyze the behavior of materials under certain stress conditions. This is often used to analyze the behavior of mechanical parts and their longevity. In this study, we attempt to use ABAQUS software to apply FEA to the stressed thin-film system.

Chapter 4: Experimental Results & Discussion

4.1 The Origins of Self-Peeling

The delamination of the Ti/Pt bilayer originates in the platinum layer and has not been observed in aluminum, gold, or titanium electrodes that are developed using the same process and parameters. The strain is caused by stresses induced during electron-beam deposition, residual stresses in the platinum film, and the thickness of the film. The Ti/Pt bilayer delaminates immediately following deposition, and the flakes often loosely adhere to the surface of the structure. They can be removed easily with some air pressure or, in some cases, by submerging the substrate in acetone and agitating it. The bilayer peels at a critical thickness once the platinum layer is approximately 95 nm thick, and the titanium adhesive layer is 5 nm. At smaller thicknesses, the bilayer is too thin, and delamination is not observed. This process is possible due to the lack of adhesion at the ODPA/Ti interface since the alkyl chain tail group of ODPA does not chemically bond with the titanium.

Electron-beam (e-beam) deposition is used to deposit the Ti and Pt films in a room temperature high-vacuum chamber. The choice of deposition method and temperature used affects the stresses induced in the films. E-beam deposition is an evaporation method that uses high energy electrons to bombard a source material so that the atoms are vaporized and launched through low background pressure to deposit onto the substrate. The temperature of the particles is thus very high and cools upon contact with the room temperature substrate. The atoms nucleate on the surface but are diffusion-limited due to the low energy. The resulting films develop residual stresses due to their amorphous

structure, and they are dependent on the properties of the source material and the interfaces between the various layers [21].

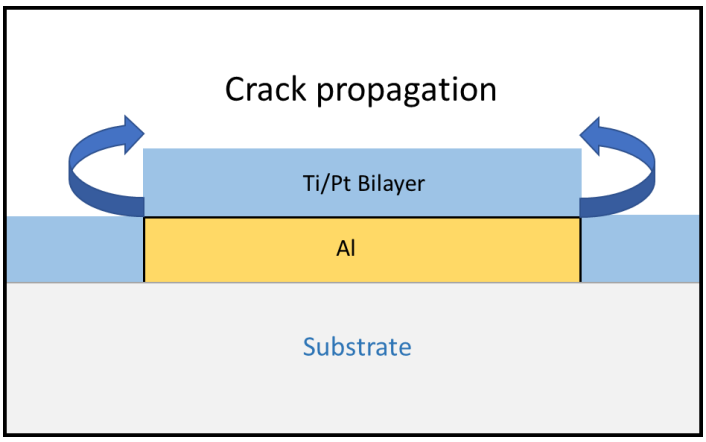

Figure 4.1: Diagram showing a more accurate profile of the deposited Ti/Pt layers and the crack propagation direction at the onset of delamination.

Due to the topography of the deposited Al and SAM layers on the substrate, the Ti/Pt layers are not level on the surface. Instead, there is height variation where the Ti/Pt is very thin at the edges of the SAM-coated Al layer as shown in the simplified diagram in Figure 4.1. This edge is often where the cracks initially develop triggering delamination.

4.2 Characterization

4.2.1 Imaging the Flakes

Initial images were taken using optical microscopy to observe the surface and the shape of the flakes on the devices. These images show clearly the Ti/Pt flakes loosely adhered to the surface of the ODPA SAM-coated Al (figure 4.2). The flakes of the large circles have dislodged likely due to their relative mass.

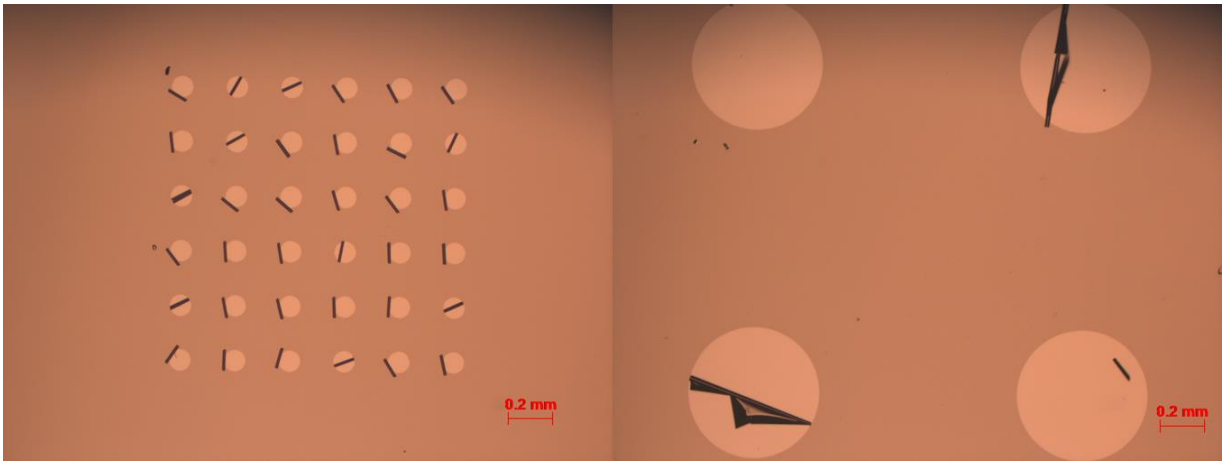

Figure 4.2: Optical micrographs of Al circles with Ti/Pt flakes rolled on the surface of 100 μm circle in the left image and 600 μm circles in the right image.

An analysis of the percentage of circles that self-peeled in two samples fabricated in different batches under the same parameters provides insight into the effect of circle size on delamination. Our mask design contains four different size circles, as shown in Figure 3.1. In one sample, 0% of the 900 μm diameter circles, 75% of the 600 μm circles, 3% of the 300 μm circles, and 78% of the 100 μm circles peeled off. These values were observed after deposition without any agitation or submersion in acetone. In another sample, 100% of the 900 μm circles, 100% of the 600 μm circles, 92% of the 300 μm circles, and 43% of the 100 μm circles peeled off. Almost all circles had flakes still loosely adhered to the surface, as shown in Figure 4.2. In most samples fabricated, the larger circles are more likely to have the flakes fall off before imaging likely due to their mass. They also tend to peel off in random crumpled patterns while smaller diameter circles, especially the 100 μm circles, are most likely to have flakes peel off in perfect rolls. The difference in the number of the circles that have peeled off and the variation

with size between the two samples analyzed represents the variation in possible results. Most often, the samples are more like the second example with nearly all the circles peeling off and the larger flakes falling off.

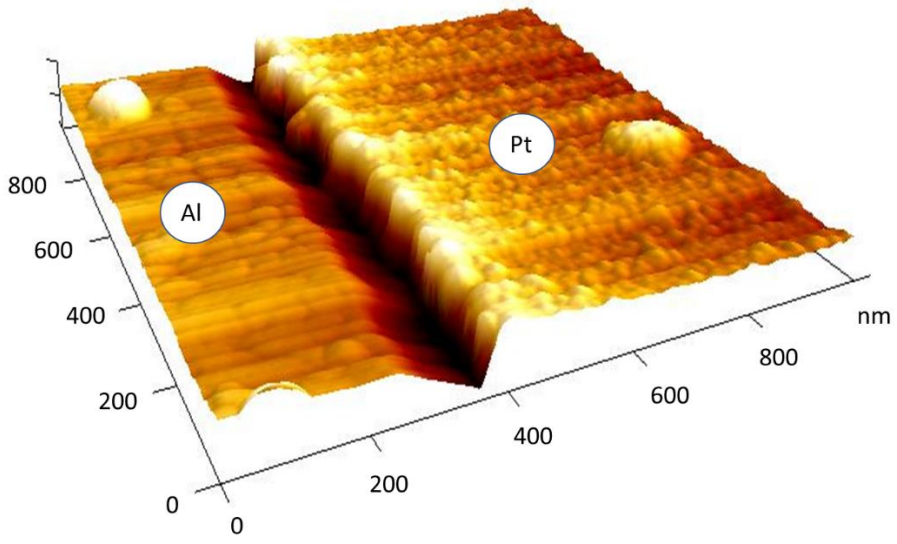

Figure 4.3: 3D AFM scan of a 1 μm^2 area at the right edge of a 600 μm circle at the nanogap between Al and Pt electrodes.

AFM allows us to look at the topographical profile at and around the nanogap. The cantilever does not reach the bottom of the gap, so the results show up to 50 nm depth in the possibly 100 nm gap depth. The image results vary whether we raster from the right or the left, from Pt to Al or from Al to Pt, respectively, due to the dip and rise of the cantilever with the gap. Figure 4.3 shows an Al-ODPA SAM-Ti/Pt system rastered at the right edge of a 600 μm circle with a whisker cantilever, which is 5° angle at the tip and angled 90 degrees with respect to the surface measured. The graphical depth profile shows the gap and an increase in height at the edge of the Pt surface likely caused by the movement of the cantilever (figure 4.4).

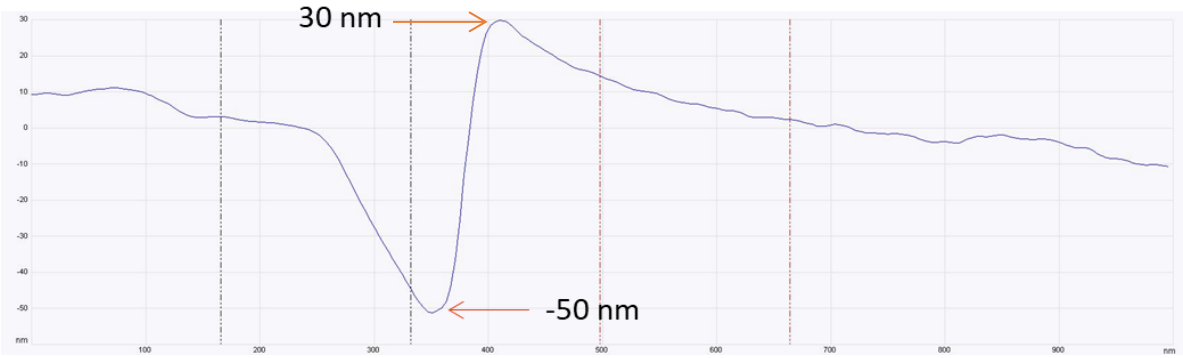

Figure 4.1: AFM graphical height profile of a 1 μm^2 area at the right edge of a 600 μm circle at the nanogap between Al and Pt electrodes.

A height profile of the same area shows the variation in height between the Al (left) and Pt (right) electrodes as only apparent initially. This supports that the edge height is an imaging artifact and likely not due to actual variation in height as both layers are deposited at 100 nm. The gap width seems to be 100 nm, but this is inaccurate as the gap cannot be accurately measured using the AFM due to the limitations of the cantilever. Similarly, the nanogap's depth is more than 50 nm but the cantilever cannot image any deeper.

Scanning electron microscope (SEM) images of the flakes provide us with a closer look into the behavior of the peeling layer due to stress and size variation. It also allows us to measure the rolling diameter for use in stress calculations. Images were taken of the 100 and 300 μm circles because the flakes of the 600 and 900 μm circles had fallen off. The nanogap itself could not be accurately imaged with the SEM due its size.

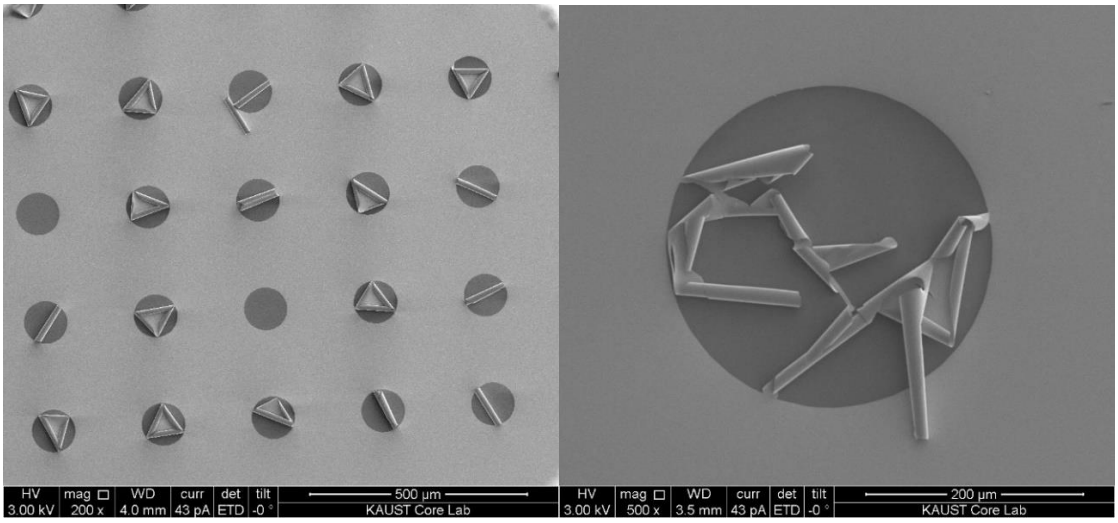

Figure 4.5: SEM images of Ti/Pt delaminated flakes on the surface of 100 µm diameter Al electrodes froming tubular and triangular structures (left) and irregular tubular flakes on 300 µm diameter Al electrodes (right).

When the Ti/Pt layer peels off, it is observed to roll into tubes or pinned tubular structures (Figure 4.5) or develop uniformly distributed cracks on the surface. The rolled films are thought to have uniform thin Ti/Pt films. The Ti atoms may diffuse into the shag-like ODPA SAM layer and pin onto the surface of the Al first metal causing the weak adherence of the flakes on the surface of the electrodes (figure 4.5). Cracking is caused by the brittleness of the metals, their nanoscale thickness, and the pinning of Ti onto the Al layer. The combination of these mechanical phenomena allows the layer to fracture. Since the films are isotropic, the cracks develop uniformly along the surface.

Differently sized structures on the substrate also affect the patterns in which the films peel off. Larger structures, such as the 900 µm diameter circles, develop more irregular structures that peel off and flake off quickly after deposition because of the increased

pinning due to the large surface area and weight of the flakes whereas smaller structures such as the 100 μm diameter circles have more uniform rolls and retain the flakes until agitated either with air or if washed with acetone.

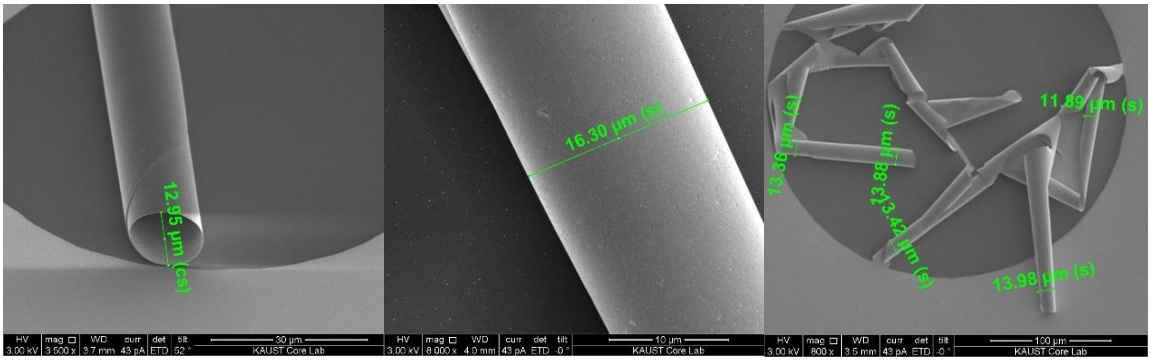

Figure 4.6: SEM measurements of the diameters of the flakes in the 100 μm and 300 μm

Scanning electron microscopy (SEM) was used to image the flakes that formed on the patterned electrodes (figure 4.6). The diameters of the flakes that formed on the 100 μm circles and the 300 μm circles, were measured and the results were collected and averaged. The diameter of the flakes is a direct measurement of the bending curvature of the Ti/Pt layer, an important parameter in the calculation of stress. The average rolling diameter of the flakes is 13.8 μm for both the 100 and 300 μm diameter circles. Such results indicate that the stress is equally distributed across the surface since it does not vary much with size. This confirms the assumption that the stress is intrinsic and develops during deposition.

4.3 Optimization

4.3.1 Platinum Critical Thickness

To determine the critical thickness of Pt at which delamination of Ti/Pt occurs, we deposited Pt at various thicknesses. Platinum films of 15, 35, 55, 75, 95, and 145 nm were deposited on six substrates. The same procedure previously described was used to create nanogaps between an Al first metal and a Ti/Pt second metal. A 5 nm layer of Ti was first deposited using e-beam evaporation on all six substrates then removed from the vacuum in preparation for the separate Pt depositions. In our original process that self-peels the Ti and Pt layers are deposited sequentially without breaking the vacuum, this may affect our results. We found that the Ti films are stable as well as the 15, 35, 55, and 75 nm Pt films, and no stress effects are observed. The 95 and 145 nm Pt samples spontaneously delaminated. The critical thickness is in the range of 95 nm, and the stress increases in the film as thickness increases.

4.3.2 Heat Cycling

The process of heat cycling to increase the stress in Al and Au films was used to increase the stress to achieve delamination in metals other than the Ti/Pt bilayer. First, samples of 100 nm Al first metal and either Al or Al/Au second metal electrodes were fabricated using the same deposition process as in Figure 2.1 without an extra peeling step so that the second metal covers the first metal and the SAM layer (table 4.1). The 5 nm Al layer in samples 1 and 2 serve the same purpose as the Ti layer in our original devices; to make sure the second metal either Pt or Au adheres to the glass substrate.

Table 4.1: Nanogap electrode combinations fabricated for the heat cycle experiment.

Sample #	Metal 1	Thickness (nm)	Interlayer	Thickness (nm)	Metal 2	Thickness (nm)	Deposition Method
1	Al gate mask	100	Al	5	Au	95	Thermal
2	Al gate mask	100	Al	5	Au	95	Thermal
3	Al gate mask	100	N/A	-	Al	100	Thermal
4	Al gate mask	100	N/A	-	Al	100	Thermal

Three heat cycles from room temperature to 310℃ were performed on a hot plate. The samples were heated at a rate of approximately 14℃/min and cooled at a rate of approximately 6℃/min. Hodge et al. showed an increase of stress by ~50 MPa in Au films and ~140 MPa for Al films deposited on a silicon substrate heated from room temperature to approximately 200°C [22]. Therefore, 310℃ should have increased the stress but not enough to cause delamination. The surface of the samples was unchanged except for some discoloration on the surface of the Au film when it became more orange. The annealing may affect the interfaces in the structure by causing them to relax. ODPA SAM has been shown to have excellent thermal stability after annealing at 400-450℃ in N_2 for 10 minutes [27]. Therefore, the heat or the Au and Al properties prevent the amount of stress necessary to bend the film.

4.4 Stress Analysis

4.3.1 FLX-2320 Stress Measurement System

The FLX Stress Measurement System in Figure 3.3 uses two lasers to scan the surface of a substrate before and after a film is deposited onto it to measure the change in the radius of curvature caused by the film. Stoney's equation is then used by the accompanying analysis software to calculate the stress in the film. Two Si calibration wafers are

provided with the system with instructions on how to perform the calibration. The results were consistent with the manual.

Due to the Ti/Pt bilayer delaminating from the surface of the substrate and forming rolls, adjustments had to be made. The goal was to measure the stress on a 4-inch wafer because that is the smallest size wafer that can be scanned in the chamber. We initially wanted to test if the Ti/Pt bilayer would delaminate from a 4-inch wafer covered completely in ODPA SAM-coated Al Since the system measures the radius of curvature relatively, the glass substrate must be initially scanned, then after 100 nm Al deposition, it must be scanned a second time. We skipped measuring the ODPA SAM since it is small and adheres to the surface in a way that it is unlikely to cause any bending due to stress. A third scan is done after the deposition of 5 nm Ti. The measurements at this point should show tensile stress, but they initially showed relatively high compressive stress. The same sample was measured four times in a row and showed wildly fluctuating values. These measurements can be seen in Table 4.2. These inconsistent results point to an error in the system. The system provider was contacted about the issue, but the error has not resolved as of the time of this publication.

Table 4.2: Stress measurement results of a glass substrate coated with 100 nm Al, ODPA SAM, and 5 nm Ti. These measurements were taken consecutively on the same device and show inconsistent results.

Measurement	Stress (MPa)
1	-219.1920 Compressive
2	-945.0693 Compressive
3	-8145.58 Compressive
4	18.0719 Tensile

4.4.2 ABAQUS Simulation

To simulate the behavior of our stressed film and quantify the stress required to induce self-peeling, ABAQUS software was used. ABAQUS uses finite elements analysis (FEA) to model mechanical systems. To model our Ti/Pt stressed system, we make two assumptions. First, we approximate that there is no adhesion at the Ti and ODPA SAM interface. In reality, there will be some adhesion, including the previously discussed pinning through the SAM. The second assumption is that the stress is entirely extrinsic and caused by a change in temperature. Since intrinsic stress can depend on many variables, it is difficult to quantify in simulation.

We used Timoshenko's equation (eq. 2) to approximate the change in temperature that corresponds to our measured radius of curvature of 6.9 μm that was obtained from the images in Figure 4.6. Timoshenko's model was used because the bimetal strip most accurately reflects our Ti/Pt bimetal film. The calculated value for effective temperature

for our system is 236474 K, which is very large. The parameters used in the calculation are provided in Table 2.1. This result is plausible because the bimetal film is subject to both intrinsic and extrinsic stress, not only extrinsic temperature change. When we assume all the stress is due to temperature change, the value will be very high.

Properties of the Ti and Pt films: Young's modulus, Poisson's ratio, CTEs, and layer thicknesses are input in the software (table 2.1). Then the initial conditions are set of a 5 nm Ti film interfaced with a 95 nm Pt film at room temperature. The 2D cross-section was taken to be 1 μm in length initially for computational speed, and the sample was sectioned into nodes. Each node represents a small section of the area over which the simulation calculations are performed. As the number of nodes increases, the simulation becomes more accurate and more computationally intensive due to the number of calculations. The student version of ABAQUS only allows up to 1000 nodes to be used in a single simulation and was not sufficient. To obtain accurate results, the simulation must be performed with enough nodes and a cross-section of 100 μm. This will require a GPU and will take time. Since the most important parameter which is the residual stress that causes the delamination of our film is replaced here with an approximated high temperature value, the resulting stress values may not accurately reflect our devices. It is more accurate and practical to find the stress value empirically.

4.4.3 Mathematical Analysis

Many mathematical models that can be used to quantify the stress in films and various film configurations. The most notable is Stoney's equation, which does not work for our system mainly due to the delamination. Timoshenko's equation is a modification on Stoney's equation for bimetallic strips and is the most applicable model for our system.

The modified Timoshenko's equation (Eq. 3) for nanoscopically thin films can be used to calculate the difference in stress between the top and bottom surfaces of the bimetals from the radius of curvature. Since the stresses for both metals are separate variables and both are unknown, the equation is impossible to solve as presented. The FEA analysis was an attempt to overcome this and calculate the stress through simulation.

Several other mathematical models were attempted for the simulation and to calculate the stress or temperature using the known radius of curvature, including the Kirchoff-Love theory and other stress equations. We used MATLAB to calculate values based on various assumptions such as assuming the Ti was the substrate and Pt was the film for Stoney's equation then assuming Al was the substrate and the Ti/Pt bilayer was the film. These calculations gave questionable results and are provided in the appendix for reference.

Chapter 5: Conclusions and Future Work

5.1 Conclusions

In this work, we discovered that nanogap co-planar electrodes of Al and Ti/Pt patterned onto a glass substrate using a-lith self-form without the need for an additional peeling step. The self-forming mechanism is due to stresses in the Ti/Pt bilayer that likely originate during e-beam deposition and cause the excess material to flake off in rolls revealing nanogaps on the order of 10 nm. This mechanism is highly desirable due to the inconsistency of results caused by external peeling mechanisms that are subject to user error. The goal of this work was to determine the origin of the stress, quantify it, and determine whether these results can be replicated using other second metal electrode materials such as Al and Au. Experimental and theoretical research was conducted to this end.

Several experiments were carried out to characterize and optimize the self-peeling mechanism. The Ti/Pt were initially deposited at 5/95 nm. To determine where the critical thickness that triggers self-peeling is, the thickness of the Pt layer was varied between 15 and 145 nm. Pt films of 95 nm and thicker were found to self-peel while thinner films did not. Heat cycling was used to attempt to induce self-peeling in Al and Au second metal electrodes by increasing the stress. Self-peeling was not observed up to 310°C. Several characterization methods were used to observe and measure the flakes and, the rolling diameter of the flakes was found to be approximately 13.8 μm using SEM.

Theoretical research shows that the stress in the films causing rolling must be tensile and previous research has shown a similar Ti/Pt bilayer with stress values of 700-800 MPa, providing us with a stress value estimate. Electron-beam deposition is a high energy process and is likely where the stress originates due to the growth mechanism and rapid cooling of the films. Mathematical models such as Stoney's and Timoshenko's equations were applied to our system but failed to provide an accurate value for the stress due to different assumptions used and the fact that the stresses are intrinsic residual stresses that are difficult to model.

Unless heating methods at higher temperatures can induce the stress required for Au or Al to self-peel, it is unlikely that this mechanism can be recreated in other metals. Subjecting the substrate to high annealing temperatures will likely affect other aspects of the device, such as the stability of the SAM and the first metal electrode. FEA simulation may still provide an approximation of the stress in the Pt film and can show us the stress required to induce rolling in other metals. This data may be useful if it can be experimentally recreated.

5.2 Future Work

To further explore the effect of deposition on the stressed Pt thin films, an experiment can be conducted where a 5 nm Ti film and a 50 nm Pt film are initially deposited. The sample would be removed from the vacuum and returned to deposit the remaining 45 nm of Pt. This experiment will provide insight as to whether the stress is due to deposition conditions or surface reconstruction and intrinsic Pt material properties.

If the stress in the Ti/Pt film is truly uniform, then it should show the same values of stress on the parts of the film that adhere to the glass substrate. If the stress measurement system can be properly calibrated, a Ti/Pt 5/95 nm bilayer can be deposited directly onto a 4” glass wafer and the stress can be measured using Stoney’s equation in the FLX Stress Measurement System or via another method of measuring the radius of curvature of the substrate such as profilometry. Another possible method of measuring the stress is nanoindentation via the AFM system.

Since e-beam evaporation is a high energy deposition method that causes more residual stress in the deposited films, depositing Au and Al second metals via e-beam may be worth exploring. Studying the stress change due to deposition method and pairing it with heat cycles to increase stress may be the extent to which stress can be increased and could possibly cause self-forming.

Heat cycling by slowly heating the samples on a hot plate may not have worked due to the speed at which the samples are heated or due to an insufficient amount of heat. Using a flash lamp to quickly heat the top surface of the second metal to higher temperatures could induce enough stress to trigger self-peeling.

REFERENCES

[1] Li, T., Hu, W., & Zhu, D. (2010). Nanogap electrodes. *Advanced Materials*, *22*(2), 286-300.

[2] Dubois, V., Bleiker, S. J., Stemme, G., & Niklaus, F. (2018). Scalable manufacturing of nanogaps. *Advanced Materials*, *30*(46), 1801124.

[3] Li, M., Bhiladvala, R. B., Morrow, T. J., Sioss, J. A., Lew, K. K., Redwing, J. M., ... & Mayer, T. S. (2008). Bottom-up assembly of large-area nanowire resonator arrays. *Nature Nanotechnology*, *3*(2), 88-92.

[4] Hobbs, R. G., Petkov, N., & Holmes, J. D. (2012). Semiconductor nanowire fabrication by bottom-up and top-down paradigms. *Chemistry of Materials*, *24*(11), 1975-1991.

[5] Luo, S., Hoff, B. H., deMello, J. C., Spontaneous Formation of Nanogap Electrodes by Self-Peeling Adhesion Lithography. *Adv. Mater. Interfaces* 2019, 6, 1900243.

[6] Beesley, D. J., Semple, J., Jagadamma, L. K., Amassian, A., McLachlan, M. A., Anthopoulos, T. D., & Demello, J. C. (2014). Sub-15-nm patterning of asymmetric metal electrodes and devices by adhesion lithography. *Nature communications*, *5*, 3933.

[7] Lee, K. N., Seo, Y. T., Lee, M. H., Jung, S. W., Kim, Y. K., Kim, J. M., & Seong, W. K. (2012). Stress-induced self-rolled metal/insulator bifilm microtube with micromesh walls. *Journal of Micromechanics and Microengineering*, *23*(1), 015003.

[8] Froeter, P., Yu, X., Huang, W., Du, F., Li, M., Chun, I., ... & Li, X. (2013). 3D hierarchical architectures based on self-rolled-up silicon nitride membranes. *Nanotechnology*, *24*(47), 475301.

[9] Shenoy, V. B., & Gracias, D. H. (2012). Self-folding thin-film materials: From nanopolyhedra to graphene origami. *Mrs Bulletin*, *37*(9), 847-854.

[10] Overman, N. R., Overman, C. T., Zbib, H. M., & Bahr, D. F. (2009). Yield and deformation in biaxially stressed multilayer metallic thin films. *Journal of engineering materials and technology*, *131*(4).

[11] Cho, J. H., James, T., & Gracias, D. H. (2010). Curving nanostructures using extrinsic stress. *Advanced Materials*, *22*(21), 2320-2324.

[12] Stoney, G. G. (1909). The tension of metallic films deposited by electrolysis. *Proceedings of the Royal Society of London. Series A, Containing Papers of a Mathematical and Physical Character*, *82*(553), 172-175.

[13] Timoshenko, S. (1925). Analysis of bi-metal thermostats. *Josa*, *11*(3), 233-255.

[14] Freund, L. B., Floro, J. A., & Chason, E. (1999). Extensions of the Stoney formula for substrate curvature to configurations with thin substrates or large deformations. *Applied Physics Letters*, *74*(14), 1987-1989.

[15] Klein, C. A. (2000). How accurate are Stoney's equation and recent modifications. *Journal of Applied Physics*, *88*(9), 5487-5489.

[16] Zang, J., & Liu, F. (2008). Modified Timoshenko formula for bending of ultrathin strained bilayer films. *Applied Physics Letters*, *92*(2), 021905.

[17] Pureza, J. M., Lacerda, M. M., De Oliveira, A. L., Fragalli, J. F., & Zanon, R. A. S. (2009). Enhancing accuracy to Stoney equation. *Applied Surface Science*, *255*(12), 6426-6428.

[18] Vos, J. G., Forster, R. J., & Keyes, T. E. (2003). *Interfacial supramolecular assemblies*. John Wiley & Sons.

[19] Smith, D. L., Wysocki, V. H., Colorado, R., Shmakova, O. E., Graupe, M., & Lee, T. R. (2002). Low-Energy Ion− Surface Collisions Characterize Alkyl-and Fluoroalkyl-Terminated Self-Assembled Monolayers on Gold. *Langmuir*, *18*(10), 3895-3902.

[20] Zang, J., Huang, M., & Liu, F. (2007). Mechanism for nanotube formation from self-bending nanofilms driven by atomic-scale surface-stress imbalance. *Physical review letters*, *98*(14), 146102.

[21] Freund, L. B., & Suresh, S. (2004). *Thin film materials: stress, defect formation and surface evolution*. Cambridge university press.

[22] Hodge, T. C., Bidstrup-Allen, S. A., & Kohl, P. A. (1997). Stresses in thin film metallization. *IEEE Transactions on Components, Packaging, and Manufacturing Technology: Part A*, *20*(2), 241-250.

[23] Flinn, P. A., Gardner, D. S., & Nix, W. D. (1987). Measurement and interpretation of stress in aluminum-based metallization as a function of thermal history. *IEEE Transactions on electron devices*, *34*(3), 689-699.

[24] Flinn, P. A. (1991). Measurement and interpretation of stress in copper films as a function of thermal history. *Journal of materials research*, *6*(7), 1498-1501.

[25] Bobb-Semple, D., Nardi, K. L., Draeger, N., Hausmann, D. M., & Bent, S. F. (2019). Area-selective atomic layer deposition assisted by self-assembled monolayers: a comparison of Cu, Co, W, and Ru. *Chemistry of Materials*, *31*(5), 1635-1645.

[26] Leng, Y. (2009). *Materials characterization: introduction to microscopic and spectroscopic methods*. John Wiley & Sons.

[27] Bashir, A., Wöbkenberg, P. H., Smith, J., Ball, J. M., Adamopoulos, G., Bradley, D. D., & Anthopoulos, T. D. (2009). High-Performance Zinc Oxide Transistors and Circuits Fabricated by Spray Pyrolysis in Ambient Atmosphere. *Advanced Materials*, *21*(21), 2226-2231.

APPENDIX

MATLAB code of the mathematical equations and the various assumptions attempted.

Contents

Constants

All the material constants needed for the calculations are predefined here:

```
   % Young's moduli
E_al = 69E9;
E_glass = 64E9;
E_ti = 113.8E9;
E_pt = 169E9;

    % Poisson's ratios
nu_al = 0.334;
nu_glass = 0.2;
nu_ti = 0.32;
nu_pt = 0.39;

    % Coefficients of thermal expansion
CTE_al = 22.5E-6;
CTE_ti = 8.7E-6;
CTE_pt = 9E-6;
CTE_glass = 3.25E-6;

    % Thicknesses (m)
t_al = 100E-9;
t_ti = 5E-9;
t_pt = 95E-9;
t_glass = 0.0011;
t_bi = 100E-9;

% Measured rolling radius (m)
R = 6.9E-6;
```

Stoney's Equation

Calculate the film stress using Stoney's equation: Stress = ((Es*(ts^2))/(6*(1-nus)*tf))*(1/R)

```
    % 1. Assuming Ti is our substrate and Pt is the film (0 adhesion to the
    % SAM)
    Stress1 = ((E_ti*(t_ti^2))/(6*(1-nu_ti)*t_pt))*(1/R);

    disp(['1. The stress in Pt = ' num2str(Stress1) ' Pa'])
```

```
% 2. Assuming Al is our substrate and Ti/Pt bilayer is our film.
Stress2 = ((E_al*(t_al^2))/(6*(1-nu_al)*t_bi))*(1/R);

disp(['2. The stress in the Ti/Pt bilayer = ' num2str(Stress2) ' Pa'])

% 3. Assuming glass is our substrate and Ti/Pt bilayer is our film.
Stress3 = ((E_glass*(t_glass^2))/(6*(1-nu_glass)*t_bi))*(1/R);

disp(['3. The stress in the Ti/Pt bilayer = ' num2str(Stress3) ' Pa'])

% 4. Assuming Pt is our substrate and Ti is the film (0 adhesion to the
% SAM)
Stress4 = ((E_pt*(t_pt^2))/(6*(1-nu_pt)*t_ti))*(1/R);

disp(['4. The stress in Ti = ' num2str(Stress4) ' Pa'])

% 1. is the only reasonable assumotion but 1 MPa is too low, according
% to literature it should be ~700-800 MPa. In Stoney, the substrate is
% much larger than the film.
```

```
1. The stress in Pt = 1063774.0985 Pa
2. The stress in the Ti/Pt bilayer = 250250250.2503 Pa
3. The stress in the Ti/Pt bilayer = 2.338164251207729e+16 Pa
4. The stress in Ti = 12079076581.9276 Pa
```

Kirchhoff-Love theory

Estimate the effective temperature using the Kirchhoff-Love theory: T = (1/R)*((ts*Estars)/(6*Estarf))*(1/((1+nuf)*CTEf-(1+nus)*CTEs))

```
% Constants:
Estar_ti = (E_ti*t_ti)/((1-nu_ti)^2);
Estar_pt = (E_pt*t_pt)/((1-nu_pt)^2);
Estar_al = (E_al*t_al)/((1-nu_al)^2);
Estar_glass = (E_glass*t_glass)/((1-nu_glass)^2);

% 1. Assuming Ti is our substrate and Pt is the film (0 adhesion to the
% SAM)
T1 = (1/R)*((t_ti*Estar_ti)/(6*Estar_pt))*(1/((1+nu_pt)*CTE_pt-(1+nu_ti)*CTE_ti));

disp(['1. The change in temperature = ' num2str(T1) ' K'])

% 2. Assuming Al is our substrate and Pt is our film.
T2 = (1/R)*((t_al*Estar_al)/(6*Estar_pt))*(1/((1+nu_pt)*CTE_pt-(1+nu_al)*CTE_al));

disp(['2. The change in temperature = ' num2str(T2) ' K'])

% 3. Assuming glass is our substrate and Pt is our film.
T3 = (1/R)*((t_glass*Estar_glass)/(6*Estar_pt))*(1/((1+nu_pt)*CTE_pt-(1+nu_glass)*CTE_
glass));

disp(['3. The change in temperature = ' num2str(T3) ' K'])

    % 4. Assuming Pt is our substrate and Ti is the film
```

```
    T4 = (1/R)*((t_pt*Estar_pt)/(6*Estar_ti))*(1/((1+nu_ti)*CTE_ti-(1+nu_pt)*CTE_pt));

    disp(['4. The change in temperature = ' num2str(T4) ' K'])
```

```
1. The change in temperature = 3.3571 K
2. The change in temperature = -49.7494 K
3. The change in temperature = 7867400116.2742 K
4. The change in temperature = -78420.9506 K
```

Timoshenko Formula

Calculate the change in temperature based on the Timoshinko formula: R = ((t_ti+t_pt)*(3*(1+m)^2 + (1+m*n)*(m^2+(1/(m*n)))))/(6*(CTE_pt-CTE_ti)*(1+m)^2*DelT);

```
% Define new variables m and n:
m = t_ti/t_pt;
n = E_ti/E_pt;

DelT = ((t_ti+t_pt)*(3*(1+m)^2 + (1+m*n)*(m^2+(1/(m*n)))))/(6*(CTE_pt-CTE_ti)*(1+m)^2*R);

disp(['The change in temperature = ' num2str(DelT) ' K'])
```

```
The change in temperature = 236474.8862 K
```

Simple formula from Xiaole

```
Simple_delT = (t_ti+t_pt)/((CTE_pt-CTE_ti)*R);

disp(['The change in temperature = ' num2str(Simple_delT) ' K'])
```

```
The change in temperature = 48309.1787 K
```

Artificial "heating temperature"

```
% A temperature-based stress used to simpliy finite element simulations
% from Kuo et al. since residual stresses are complicated and difficult to
% simulate.

% If we add together the constants of the two films (which is not specified
% in the paper).
Art_T = (750E6*(1-(nu_ti+nu_pt)))/((CTE_ti+CTE_pt)*(E_ti+E_pt));

disp(['The estimated artificial heating temperature = ' num2str(Art_T) ' K'])
```

```
The estimated artificial heating temperature = 43.4517 K
```